Construction of embedded-atom-method interatomic potentials for alkaline metals (Li, Na, and K) by lattice inversion*

Yuan Xiao-Jian(袁晓俭)[a)†], Chen Nan-Xian(陈难先)[a)b)], and Shen Jiang(申 江)[a)]

[a)] *Institute for Applied Physics, University of Science and Technology Beijing, Beijing* 100083, *China*
[b)] *Department of Physics, Tsinghua University, Beijing* 100084, *China*

(Received 8 August 2011; revised manuscript received 24 October 2011)

The lattice-inversion embedded-atom-method interatomic potential developed previously by us is extended to alkaline metals including Li, Na, and K. It is found that considering interatomic interactions between neighboring atoms of an appropriate distance is a matter of great significance in constructing accurate embedded-atom-method interatomic potentials, especially for the prediction of surface energy. The lattice-inversion embedded-atom-method interatomic potentials for Li, Na, and K are successfully constructed by taking the fourth-neighbor atoms into consideration. These angular-independent potentials markedly promote the accuracy of predicted surface energies, which agree well with experimental results. In addition, the predicted structural stability, elastic constants, formation and migration energies of vacancy, and activation energy of vacancy diffusion are in good agreement with available experimental data and first-principles calculations, and the equilibrium condition is satisfied.

Keywords: interatomic potential, embedded-atom method, Chen–Möbius lattice inversion, alkaline metal

PACS: 34.20.Cf, 61.66.Bi, 68.35.Md, 61.72.jd **DOI:** 10.1088/1674-1056/21/5/053401

1. Introduction

It has been reported that the fracture studies of quasicrystals require samples with at least several million atoms[1] and diffusion studies require simulation times at the nanosecond scale.[2] Such large sizes and long simulation times in the simulation of molecular dynamics are achievable only with classical interatomic potentials since *ab initio* simulations are limited to a few hundred atoms and a picosecond time scale.[3] However, the high fidelity of atomistic simulations is based on the exact description of interatomic interactions in materials. It, therefore, is desirable to extract accurate interatomic potentials directly from first-principles calculations. Although it is very difficult, Carlsson *et al.*[4−6] and Chen *et al.*[7−15] have successfully generated an interatomic pair-potential model from the energy curves calculated by using the density functional theory (DFT).

It is well-known that a pair-potential model causes some incorrect predictions,[16] such as a zero value for the Cauchy discrepancy ($c_{12}-c_{44}=0$ for cubic crystals) and equivalence between cohesive energy and formation energy of unrelaxed vacancy, due to its internal deficiency, which fails to describe the dependence of bond energy on the local bonding environment. Since the 1980s, a variety of interatomic many-body potentials, which distinctly or implicitly describe the impact of other bonds on the strength of one bond, have been derived from fundamental considerations or by empirical methods, such as the embedded-atom-method (EAM) potential[17,18] and the N-body (or F–S) potential[19] for metallic systems, as well as the Stillinger-Weber potential,[20] the Tersoff potential,[21] and the bond-order potential[22] for covalent materials. Among them, the EAM formalism has drawn the most extensive attention and effort from the physical community.

In earlier studies,[18,23−28] all or most of the functions constituting the EAM potential are parameterized by prechoosing analytic forms containing potential parameters, which are fitted to the experimental values of equilibrium lattice parameter, cohesive energy, three elastic constants, and unrelaxed vacancy formation energy. For a noncubic material, this data set includes additional elastic constants and equilib-

*Project supported by the National Basic Research Program of China (Grant No. 2011CB606401).
†Corresponding author. E-mail: xjyuan10@foxmail.com
© 2012 Chinese Physical Society and IOP Publishing Ltd

rium axial ratio. Since these experimental properties represent the behaviour of materials in the immediate vicinity of an equilibrium crystal configuration in configuration space, the EAM potential generally gives a poor prediction of properties and even produces inaccurate forces during the molecular dynamics simulations for a larger range in configuration space.

In order to improve accuracy and transferability, a cubic spline-based EAM potential[3,29−34] was further developed by using first-principles calculations. All functions constituting the EAM potential are parameterized by cubic splines. The spline knots are fitted to a large number of forces on individual atoms, energy per atom, and stress, which are calculated by using DFT at different temperatures for a large number of atomic configurations with different geometries (such as defects, adatoms and surfaces, slabs, layers, atomic chains, clusters, molecules, crystals with a variety of structures, and liquids), and experimental data. However, performing computations on a very large number of forces, energy, and stress is very time-consuming.

Four years ago, Baskes *et al.*[35] proposed a new method for building the modified embedded-atom-method (MEAM)[36] potential based on the *ab initio* reference database. Almost all the MEAM functions can be determined by the multistate, which includes reference structures and reference paths, and thus this potential model was named multistate MEAM (MS-MEAM). The metal Cu was chosen as an example and extensive predictions of the MS-MEAM potential were made. However, some of the results were not quantitatively consistent with experiment data. It is not clear whether this disagreement is due to a deficiency in the MS-MEAM formalism or in the *ab initio* reference database.

Recently, following Baskes, some authors[37] have presented a physically reliable universal method of acquiring atomic electron density (AED) and pair-potential functions in the EAM formalism from first-principles calculations by using the Chen–Möbius lattice inversion.[7,8] By parameterizing the universal form of embedding energy-electron density curves in homogeneous electron gas as the embedding function, a new procedure is developed for building the EAM interatomic potential for metals with fcc, bcc, and hcp structures. On the basis of first-principles calculations, this new version of the EAM potential, named the lattice-inversion embedded-atom-method (LI-EAM) potential, eliminates all the prior arbitrary choices in the determination of AED and pair-potential functions, and minimizes the arbitrariness that generally exists in the construction of almost all the interatomic potentials.

Up to now, there have been only a few classical interatomic potentials for alkaline metals, and they are not satisfactory. With the MEAM potential[36] as an example, the predicted order of low-index surface energy among Li, Na, and K metals is not consistent with experimental information.[38,39] The low-index surface energies predicted with the AEAM potnetial[40] and the MAEAM potential[41] for alkaline metals are much smaller than experimental data. In addition, the alkali metals are of special interest for comparison with different theoretical models in condensed matter physics, particularly because of their simple electronic structure with only one conduction electron outside the closed-shell configurations. Therefore, it is necessary to construct accurate interatomic potentials for alkaline metals.

It is the purpose of this paper to extend the LI-EAM interatomic potential to alkaline metals including Li, Na, and K. We find that interatomic interactions between neighbor atoms at appropriate distances play a key role in constructing accurate EAM potential, especially for the prediction of surface energy. The constructed angular-independent potentials remarkably improve the accuracy of predicted surface energies, which agree very well with the experimental data.

In addition, we introduce how to apply the Chen–Möbius lattice inversion to obtain AED and pair-potential functions. We also describe the way to calculate the background electron density by using DFT to obtain the AED function by using the Chen–Möbius lattice inversion. In Section 4, we construct the LI-EAM potentials for Li, Na, and K. Next, these potentials are employed to predict the basic properties of Li, Na, and K to verify their reliability. Finally, we end with a conclusion.

2. Methodology

Daw[42] has shown that the form of the EAM function of a monatomic material directly follows DFT. In the Jth-neighbor model (JNM) considering interatomic interactions up to the Jth-neighbor atoms, the cohesive energy per atom of a monatomic crystal is given in the following EAM formalism:

$$E = F(\rho) + \frac{1}{2}\sum_{m=1}^{J} Z_0(m)\phi(r_m), \qquad (1)$$

$$\rho = \sum_{m=1}^{J} Z_0(m) f(r_m), \tag{2}$$

where $F(\rho)$ is the embedding energy, $\phi(r)$ is the pair potential, ρ is the background electron density of a reference atom contributed by all other atoms, $f(r)$ is the AED distribution, r_m is the distance between the mth-neighbor atoms and the reference atom at the origin, and $Z_0(m)$ is the number of the mth-neighbor atoms.

There is no doubt that a physically reliable method of the acquiring three basic functions, $F(\rho)$, $\phi(r)$, and $f(r)$, is very important for constructing accurate EAM potentials. Let us begin with the embedding function $F(\rho)$.

Banerjea *et al.*[43] deduced the universal form of embedding energy-electron density curves calculated within the density-functional scheme for homogeneous electron gas, which were made by Puska *et al.*[44] and Scott *et al.*[45] As an approximate modification caused by the heterogeneity of electron gas in the vicinity of the reference atom due to all other atoms, we parameterize this universal form

$$F(\rho) = -F_0[1 - n\ln(\rho/\rho_e)](\rho/\rho_e)^n \tag{3}$$

as the embedding function in the EAM formalism. Here the fitting parameters F_0 and n represent the parametrization, and ρ_e takes the equilibrium value of the background electron density of a reference structure (i.e., bcc structure for the alkaline metals)

$$\rho_e = \sum_{m=1}^{J} Z_0(m) f(r_{me}), \tag{4}$$

where r_{me} is the distance between the m-th neighbor atoms and the reference atom at the equilibrium reference structure.

When the uniform expansion or contraction of crystal occurs, Eqs. (1) and (2) become

$$E(r) = F[\rho(r)] + \frac{1}{2}\sum_{m=1}^{J} Z_0(m)\phi(d_0(m)r), \tag{5}$$

$$\rho(r) = \sum_{m=1}^{J} Z_0(m) f(d_0(m)r). \tag{6}$$

Thus,

$$2\{E(r) - F[\rho(r)]\} = \sum_{m=1}^{J} Z_0(m)\phi(d_0(m)r). \tag{7}$$

Here r is the first-neighbor distance under homogeneous deformation, and $d_0(m)$ is the ratio of the mth-neighbor distance to the first-neighbor distance. We extend the set $\{d_0(m)\}$ into a multiplicative semigroup $\{d(m)\}$ so that, for any two integers i and j, there always exists an integer k satisfying

$$d(i)d(j) = d(k). \tag{8}$$

Therefore, equations (6) and (7) are equivalent to the following equations:

$$\rho(r) = \sum_{m=1}^{+\infty} Z(m) f(d(m)r), \tag{9}$$

$$2\{E(r) - F[\rho(r)]\} = \sum_{m=1}^{+\infty} Z(m)\phi(d(m)r), \tag{10}$$

with

$$Z(m) = \begin{cases} Z_0(d_0^{-1}[d(m)]), & d(m) \in \{d_0(m)\}, \\ 0, & d(m) \notin \{d_0(m)\}. \end{cases} \tag{11}$$

According to the Chen–Möbius lattice inversion[7,8] the atomic electron density and pair-potential functions can be expressed as follows:

$$f(r) = \sum_{k=1}^{+\infty} I(k)\rho(d(k)r), \tag{12}$$

$$\phi(r) = 2\sum_{k=1}^{+\infty} I(k)\{E[d(k)r] - F(\rho[d(k)r])\}, \tag{13}$$

where $I(k)$, the generalized Möbius function or the inversion coefficient, can be written as

$$\sum_{d(k)|d(m)} I(k) Z\left(d^{-1}\left[\frac{d(m)}{d(k)}\right] r\right) = \delta_{m1}. \tag{14}$$

The background electron density $\rho(r)$ in Eq. (12) and the cohesive energy per atom $E(r)$ in Eq. (13) can be obtained directly from first-principles calculations. The latter can also be derived from the universal equation of state by Rose *et al.*[46] since it is, to a certain extent, based on *ab initio* calculations[4,47,48] and experimental observations,[49–53] i.e.,

$$E(r) = -E_c[1 + r^* - f_3^*(r^*)^3]\exp(-r^*), \tag{15}$$

with

$$r* = \eta(r/r_{1e} - 1), \tag{16}$$

$$\eta = \sqrt{9\Omega_e B/E_c}, \tag{17}$$

where $f_3^* = -0.05$, Ω_e is the equilibrium atomic volume, B is the bulk modulus, and E_c is the sublimation energy.

Although f_3^* in Eq. (15) equals -0.05 from the thermal expansion of Cu, this value is considered to

be suitable for almost all metals in the calculations on the derivative of bulk modulus with pressure in Ref. [46]. This was also noticed by Li *et al.*[54] and the calculated data on the pressure derivative of bulk modulus were used by Wadley *et al.*[55]

Obviously, the model parameters F_0 and n in Eq. (3) are physically demanded to be capable of fitting to the Cauchy discrepancy purely rooting in many-body interactions. In the EAM formalism, the elastic constants at equilibrium are given by[18]

$$\Omega_{\rm e} c_{ijkl} = B_{ijkl} + F'(\rho_{\rm e}) W_{ijkl} + F''(\rho_{\rm e}) V_{ij} V_{kl}, \quad (18)$$

where B_{ijkl}, W_{ijkl}, and V_{ij} take the following forms:

$$\begin{aligned} B_{ijkl} &= \frac{1}{2} \sum_{m=1}^{J} \sum_{l=1}^{Z_0(m)} \frac{r^{(l)}_{mi\,\rm e} r^{(l)}_{mj\,\rm e} r^{(l)}_{mk\,\rm e} r^{(l)}_{ml\,\rm e}}{(r_{me})^2} \\ &\quad \times \left[\phi''(r_{me}) - \frac{\phi'(r_{me})}{r_{me}} \right], \\ W_{ijkl} &= \sum_{m=1}^{J} \sum_{l=1}^{Z_0(m)} \frac{r^{(l)}_{mi\,\rm e} r^{(l)}_{mj\,\rm e} r^{(l)}_{mk\,\rm e} r^{(l)}_{ml\,\rm e}}{(r_{me})^2} \\ &\quad \times \left[f''(r_{me}) - \frac{f'(r_{me})}{r_{me}} \right], \quad (19) \\ V_{ij} &= \sum_{m=1}^{J} \sum_{l=1}^{Z_0(m)} \frac{r^{(l)}_{mi\,\rm e} r^{(l)}_{mj\,\rm e}}{r_{me}} f'(r_{me}), \quad (20) \end{aligned}$$

where $r^{(l)}_{mi\,\rm e}$ is the i-th component of the position vector from the reference atom to the l-th atom of the m-th neighbor atom at equilibrium. Moreover, the Cauchy discrepancy for cubic metals is expressed as

$$c_{12} - c_{44} = (V_{11})^2 F''(\rho_{\rm e})/\Omega_{\rm e}. \quad (21)$$

According to Eqs. (3) and (21), F_0 and n are physically required to satisfy the following equation of model parameter for cubic metals:

$$\Omega_{\rm e}(c_{12} - c_{44}) = \frac{(V_{11})^2}{\rho_{\rm e}^2} n^2 F_0. \quad (22)$$

This indicates that F_0 can be expressed in terms of n, and n can be determined by fitting to the structural energy difference, such as $E_{\rm fcc}$–$E_{\rm bcc}$ for Li, Na, and K.

Note that the so-called "JNM" implies that the cutoff distance $r_{\rm c}$ can be expressed as

$$r_{\rm c} = r_{J\rm e} + k_{\rm c}(r_{(J+1)\rm e} - r_{J\rm e}) \,,\ 0 < k_{\rm c} < 1, \quad (23)$$

where $k_{\rm c}$ is an adjustable parameter. To a certain extent, the value of $k_{\rm c}$ may be able to contribute to the structural stability. In the 4th-neighbor model (4NM), the values of $k_{\rm c}$ are listed in Table 1 for Li, Na, and K. Moreover, $\phi(r)$ and $f(r)$ are truncated at $r_{\rm c}$ as carried out by Baskes.[56]

Table 1. The potential parameters of the LI-EAM potentials for Li, Na, and K.

Metal	JNM	n	F_0/eV	$f_{\rm e}/10^{-3}$ Å^{-3}	β	$k_{\rm c}$
Li	4NM	0.2997	1.073446	1.196274	5.07648	0.15
Na	4NM	0.4074	0.585021	0.530026	6.23427	0.15
K	4NM	0.3988	0.536168	0. 231400	7.42667	0.15

For convenience, such a new type of EAM potential with atomic electron density and pair-potential functions obtained by the Chen–Möbius lattice inversion, is called the lattice-inversion embedded-atom-method (LI-EAM) potential.

3. Calculation of background electron density

The background electron density ρ for Li, Na, and K can be calculated with the help of a 2×2×2 supercell, as shown in Fig. 1, which is constructed by stacking eight conventional cells to a parallelepiped where the reference atom at the central site C is taken out.

We calculate the electron density distribution for the periodic system, which is formed by the translation of a supercell, by using the generalized gradient approximations (GGA) implemented in the CASTEP code.[57] The norm-conserving pseudopotentials for Li, Na, and K are used in this work. The plane-wave basis sets with the cutoff energies of 450 eV for Li metal, 700 eV for Na metal, and 400 eV for K metal are applied. The k-mesh points in the irreducible Brillouin zone are generated with parameters 3×3×3 for Li metal, 2×2×2 for Na and K metals by the Monkhorst–Pack scheme.[58] The energy tolerance for self-consistent field convergence is 2×10^{-6} eV per atom for all the calculations.

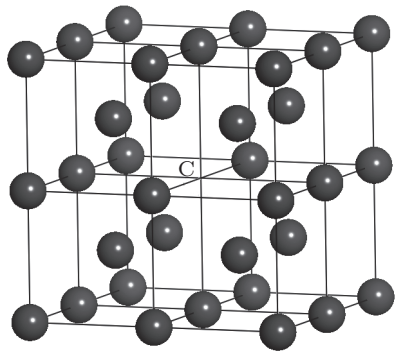


Fig. 1. The 2×2×2 supercell for calculation of the background electron density for Li, Na, and K alkaline metals.

It should be emphasized that the electron density at the central site C in the supercell is the background electron density to be calculated. We display the calculated background electron density under homogeneous deformation in Fig. 2(a) for Li metal, 2(b) for Na metal, and 2(c) for K metal. The atomic volume ranges about from half to twice of the equilibrium value. It is shown that the background electron density decreases exponentially with increasing first-neighbor distance, i.e.,

$$\rho(r) = \rho_{\rm e} \exp\left[-\lambda\left(\frac{r}{r_{1\rm e}} - 1\right)\right], \tag{24}$$

where r is the first-neighbor distance under homogeneous deformation, and the values of $\rho_{\rm e}$ and λ for Li, Na, and K metals are listed in Table 2.

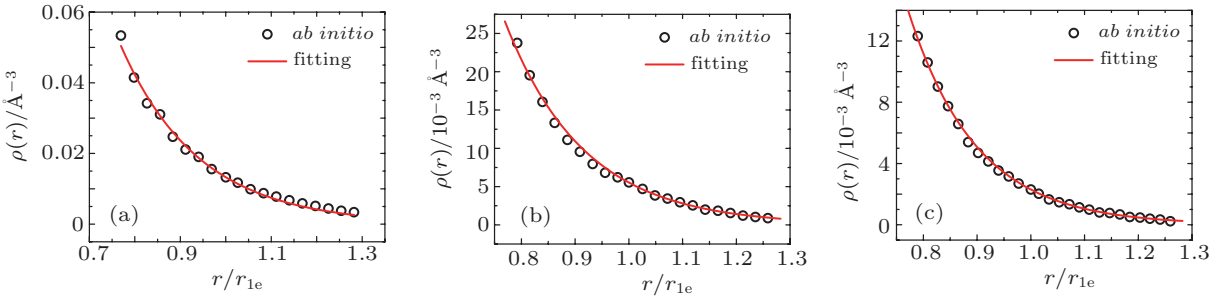


Fig. 2. (colour online) The background electron density calculated under homogeneous deformation for (a) Li metal, (b) Na metal, and (c) K metal.

Table 2. The input parameters for Li, Na, and K metals.

Metal	$\rho_{\rm e}/10^{-2}$Å^{-3}	λ	a/Å	$E_{\rm c}$/eV	B/GPa	$c_{12}-c_{44}$/GPa	$E_{\rm fcc}-E_{\rm bcc}$/eV per atom
Li	1.3276204	5.78665	3.5092[a)]	1.63[b)]	12.127[c)]	2.66[c)]	0.021[d)]
Na	0.55282759	6.81035	4.2906[a)]	1.113[b)]	6.61[c)]	2.03[c)]	0.036[d)]
K	0.23020576	7.90493	5.32[a)]	0.934[b)]	3.3267[c)]	1.26[c)]	0.028[d)]

[a)]Ref. [59], [b)]Ref. [60], [c)]Ref. [61], [d)]Ref. [27].

Table 3. The calculated background electron densities for 2×2×2 supercell compared with that for 3×3×3 supercell.

Metal	Supercell	$r/r_{\rm e}$	$\rho_{\rm e}$/Å^{-3}	Difference/%
Li	2×2×2 (including 15 atoms)	1.00	0.0133	1.5
	3×3×3 (including 53 atoms)	1.00	0.0135	
Na	2×2×2 (including 15 atoms)	1.00	0.00553	3.2
	3×3×3 (including 53 atoms)	1.00	0.00535	
K	2×2×2 (including 15 atoms)	1.00	0.00230	1.3
	3×3×3 (including 53 atoms)	1.00	0.00227	

Finally, we compare the calculated background electron densities for the 2×2×2 supercell with that for the 3×3×3 supercell, as shown in Table 3. We find that the differences between both of them for Li, Na, and K metals are all less than 5%. According to Eq. (3), we deduce that the difference of embedding energy, which is caused by the difference of background electron density, is less than 10^{-3} eV. Almost all the values of basic properties such as cohesive energy, structural energy difference, formation and migration energies of vacancy, activation energy of vacancy diffusion, surface energy, and latent heat of

melting, are about 10^{1}–10^{-3} eV. Therefore the 2×2×2 supercell is large enough so that it behaves, to a certain extent, in the same way as an infinitely large host consisting of all atoms except for the reference atom in the crystal. In fact, the atoms around the central site C up to the fifth neighbor for Li, Na, and K metals are perfectly included in the periodic system.

4. Acquisition of interatomic potential

The input parameters for the construction of the LI-EAM potentials are listed in Table 2 for Li, Na, and K metals. In the present work, for simplicity, $E(r)$ in Eq. (13) is represented by the universal function (Eq. (15)) instead of being obtained directly from first-principles calculations.

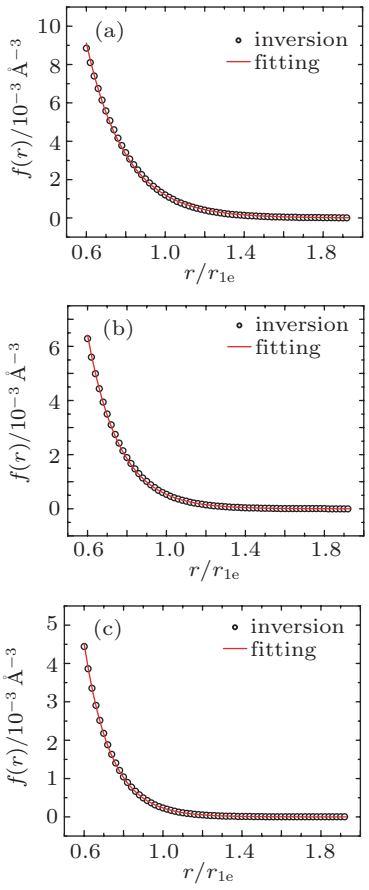


Fig. 3. (colour online) The inverted atomic electron density curves in 4NM for (a) Li metal, (b) Na metal, and (c) K metal.

The atomic electron density function can be obtained by the Chen–Möbius lattice inversion, as shown in Eq. (12). In 4NM, for instance, the inverted atomic electron densities for Li, Na, and K metals are presented in Fig. 3. The calculated results represented by the solid curves obey the following exponential decay function:

$$f(r) = f_{\rm e} \exp\left[-\beta\left(\frac{r}{r_{1\rm e}} - 1\right)\right], \qquad (25)$$

where the values of $f_{\rm e}$ and β for Li, Na, and K metals are listed in Table 1.

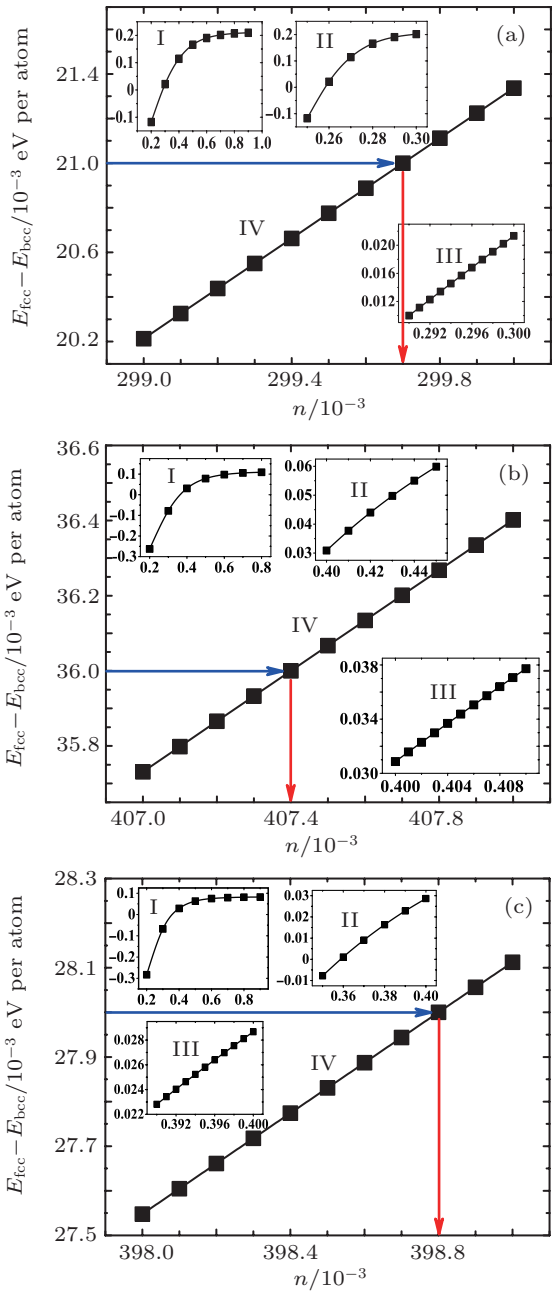


Fig. 4. (colour online) The structural energy difference $E_{\rm fcc} - E_{\rm bcc}$ versus the model parameter n calculated by 4NM for (a) Li metal, (b) Na metal, and (c) K metal.

Given a value of the model parameter n, the model parameter F_0 can be determined with Eq. (23) and the pair-potential function can be obtained with Eq. (13). Consequently, the structural energy difference can be calculated by using the LI-EAM potential.

We find that the structural energy difference varies monotonously with the model parameter n. Thus, the model parameters F_0 and n can be determined as follows.

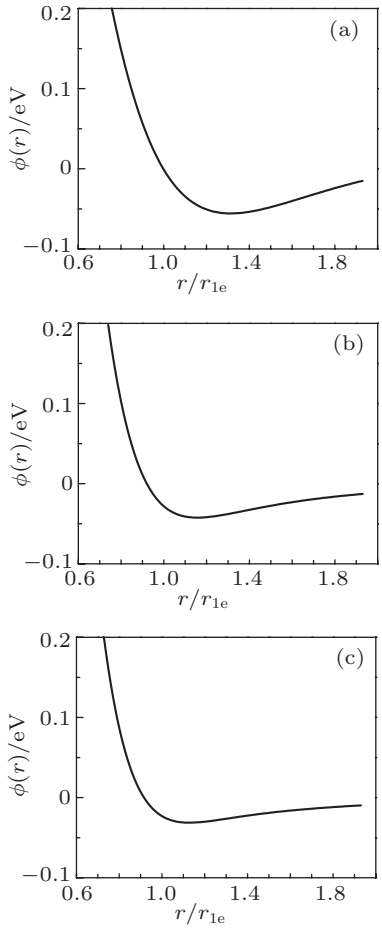


Fig. 5. The inverted pair potentials in 4NM for (a) Li metal, (b) Na metal, and (c) K metal.

Take 4NM as an example, the dependence of the structural energy difference $E_{\rm fcc} - E_{\rm bcc}$ on the model parameter n for Li, Na, and K metals are displayed in Fig. 4. In Fig. 4(a), curve I shows that the model parameter n corresponding to a structural energy difference of 0.021 eV per atom for Li metal from Table 2, is in a range of 0.25–0.3, the curve II indicates that the model parameter n is in a range of 0.29–0.3, curve III further demonstrates that the model parameter n is in a range of 0.299–0.3, and curve IV eventually confirms that the model parameter n is 0.2997 for Li metal. According to the values of $E_{\rm fcc} - E_{\rm bcc}$ in Table 2, in the same way as above, we have eventually confirmed that the values of n are 0.4074 and 0.3988 for Na and K metals, respectively. From Eq. (23), the corresponding values of the model parameter F_0 are 1.073446, 0.585021, and 0.536168 eV for Li, Na, and K metals, respectively. Consequently, the corresponding pair-potential functions can be obtained by Chen–Möbius lattice inversion expressed by Eq. (13), and are presented in Fig. 5.

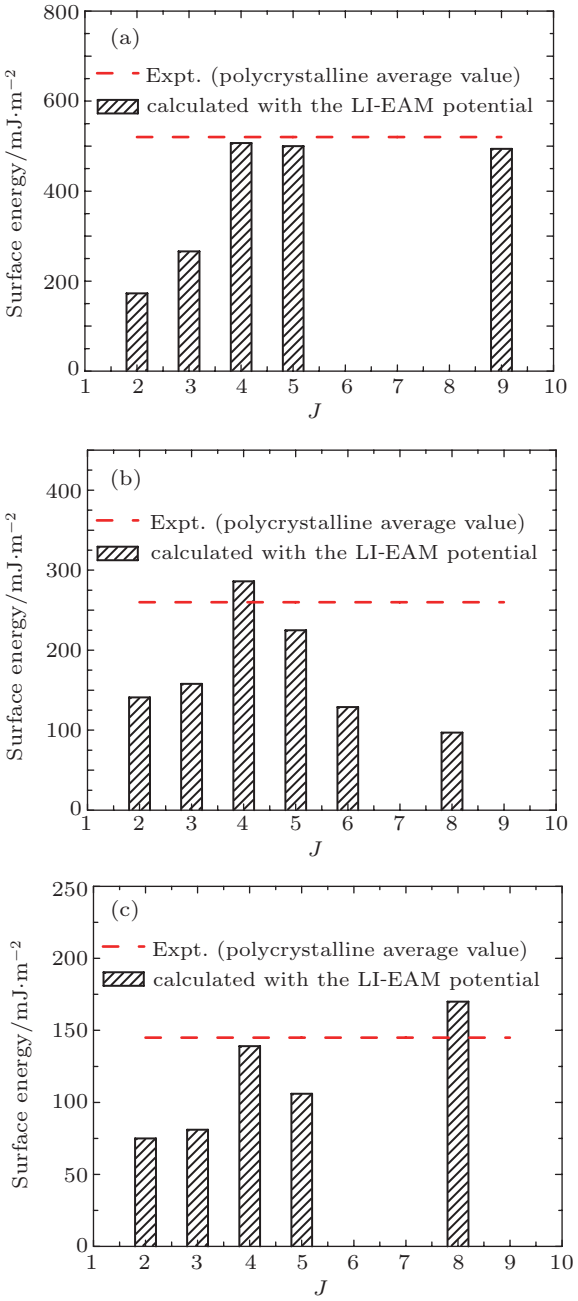


Fig. 6. (colour online) The (110) surface energies calculated by various reasonable neighbor models for (a) Li metal, (b) Na metal and (c) K metal.

Finally, we have investigated in detail the impacts of different neighbor models (from 2NM to 9NM) on the basic properties. We find that the impacts are very complicated. Whatever the value of model parameter n is in an adjustable range, structural instability always occurs in 7NM for Li, Na, and K metals. Fitting to the value of the structural energy difference

$E_{\rm fcc} - E_{\rm bcc}$ in Table 2 is carried out at the cost of losing good descriptions of other properties in 6NM and 8NM for Li metal, in 9NM for Na metal, and in 6NM and 9NM for K metal. The discrepancy of the calculated surface energies for reasonable neighbor models is significant and the (110) surface are shown in Fig. 6 as an example. The results indicate that 4NM is the most suitable for Li, Na, and K metals.

As stated above, we have constructed the LI-EAM potentials for Li, Na, and K metals, and their potential parameters are listed in Table 1. As we expected, these potentials can perfectly reproduce the values of the input parameters a, $E_{\rm c}$, B, $c_{12} - c_{44}$, and $E_{\rm fcc} - E_{\rm bcc}$ in Table 2.

5. Prediction of basic properties and discussion

Above all, we calculate the surface energy as a response to the introduction in Section 1. The low-index surface energies predicted by the LI-EAM potentials constructed here and with first-principles,[62] and the experimental polycrystalline average values[63] are presented in Table 4 for Li, Na, and K. Since there is only indirect comparison between experimental results and the present calculations, some calculations with other potentials[36,40,41] are also displayed in this table, where the underlined values are relaxed. Foiles[64] proved that the relaxation would only result in a minor reduction to the surface energy and would not markedly affect the calculation results. Therefore, we only calculate the unrelaxed surface energy as one did in Refs. [19], [25], [36], [65], and [66].

In general, the surface energies calculated with angular-independent potentials such as FBD-EAM,[23] AEAM,[25,40] FM-EAM,[33,34] MAEAM,[41,67–70] F–S,[71] LREPm,[65] and PFP[66] are much smaller than experimental data. It is encouraging that the angular-independent LI-EAM potentials constructed here drastically improve the accuracy of the predicted surface energies, which match well with experimental results.

Table 4. The low-index surface energies predicted by various potentials and first-principles and the relevant experimental data.

Method	Li/mJ·m^{-2}			Na/mJ·m^{-2}			K/mJ·m^{-2}		
	(111)	(100)	(110)	(111)	(100)	(110)	(111)	(100)	(110)
LI-EAM	507	482	507	302	287	286	148	142	139
Expt.[a]		520[f]			260[f]			145[f]	
ab initio[b]	590	522	556	287	264	253	152	142	135
AEAM[c]	–	<u>282</u>	<u>231</u>	–	<u>154</u>	<u>138</u>	–	<u>97</u>	<u>88</u>
MAEAM[d]	<u>264</u>	<u>215</u>	<u>203</u>	<u>162</u>	<u>138</u>	<u>127</u>	<u>106</u>	<u>92</u>	<u>83</u>
MEAM[e]	279	431	202	202	288	169	125	182	110

[a] Ref. [63], [b] Ref. [62], [c] Ref. [40], [d] Ref. [41], [e] Ref. [36], [f] average value

It must be pointed out that, as shown below, the drastic promotion of surface energy does not require unrealistic high values of vacancy formation energy. It is noteworthy that the surface energies of (111), (100), and (110) surfaces, which are predicted with the LI-EAM potentials in 3NM, are 303, 272, and 266 mJ/m^2 for Li metal, 180, 160, and 158 mJ/m^2 for Na metal, and 93, 86, and 81 mJ/mm^2 for K metal. The predicted results are close to the experimental results to the same extent as that with MAEAM,[41] where interatomic interactions were also considered up to the third-neighbor atoms. This indicates that the promotion of surface energy is mainly due to the considered interatomic interactions up to neighbor atoms of appropriate distance, such as the fourth neighbor atoms for Li, Na and K metals. Moreover, the drastically promoted accuracy of the predicted surface energy is also found by using the LI-EAM potentials for Fe,[37] V, Nb, and Ta metals.

From Table 4, it can be seen that the surface energies predicted in this paper are the closest to experimental results among all angular-independent potentials, and are close to experimental results to the same extent as that calculated with angular-dependent MEAM potentials. However, the (111) surface energies predicted with MEAM potentials are smaller than the predicted (100) surface energies, which is contrary to the experimental information.[38,39] Furthermore, it

has been reported[33,35,72−74] that angular-dependent potentials are much slower than angular-independent potentials in a MD simulation.

The point defect closely relates to the atom migration in materials and plays an important role in diffusion. By using the LI-EAM potential, it is very easy to calculate the formation and migration energies of a vacancy. The activation energy for self-diffusion by the vacancy mechanism is the sum of the formation and migration energies. The migration energy for a vacancy is the energy difference between atoms at the saddle point and the equilibrium site as an atom moves from the crystal site to the nearest vacant site. Table 5 displays the LI-EAM potential results, first-principles calculations,[80,81] and experimental measurements[76−79,82−85] of the formation and migration energies of vacancy and activation energy of vacancy diffusion for Li, Na, and K. Owing to the dispersivity of experimental data of vacancy formation energy, some results with other potentials[36,40,41,75] are also listed in this table, where the values denoted by an asterisk are used for fitting to their potential parameters and underlined values are relaxed. As one did in other literatures,[19,25,36,66] we only calculate the unrelaxed vacancy-formation energy since the relaxation results in only a minor reduction to the vacancy-formation energy and does not markedly affect the calculation results.[35,40,41,67−70,86] From this table, it can be also seen that the predicted formation and migration energies of vacancy and the activation energy of vacancy diffusion are in satisfactory agreement with the experimental data or first-principles calculations.

Table 5. The predicted formation energy $E^{\rm f}_{\rm 1v}$ and migration energy $E^{\rm m}_{\rm 1v}$ of vacancy and activation energy $Q^{\rm a}_{\rm 1v}$ of vacancy diffusion in comparison with the experimental data and calculation results with other potentials.

Metal	$E^{\rm f}_{\rm 1v}$/eV	$E^{\rm m}_{\rm 1v}$/eV	$Q^{\rm a}_{\rm 1v}$/eV	Method
	0.56	0.021	0.58	LI-EAM
	0.334[e];0.48[f];0.57[g]	0.038[f]	0.52[h]	Expt.
	0.53[i]	0.055[i];0.073[j]		*ab initio*
Li	0.42*(0.40)	0.11	0.53(0.51)	AEAM[a]
	0.34*	–	–	MEAM[b]
	0.414*(0.336)	0.131	0.545(0.467)	MAEAM1[c]
	0.48*	0.0361	0.516	MAEAM2[d]
	0.53	0.082	0.61	LI-EAM
	0.271[k];0.34[f];0.46[l]	0.03[f]		Expt.
	0.34[i]	0.054[i];0.076[j]		*ab initio*
Na	0.38*(0.36)	0.09	0.47(0.45)	AEAM[a]
	0.42*	–	–	MEAM[b]
	0.360*(0.297)	0.100	0.460(0.397)	MAEAM1[c]
	0.34*	0.035	0.375	MAEAM2[d]
	0.40	0.070	0.47	LI-EAM
	0.34[f];0.4[m];0.42[n]	0.038[f]		Expt.
	0.30[i]	0.051[i];0.070[j]		*ab initio*
K	0.38*(0.36)	0.09	0.47(0.45)	AEAM[a]
	0.42*	–	–	MEAM[b]
	0.360*(0.296)	0.097	0.457(0.393)	MAEAM1[c]
	0.34*	0.052	0.392	MAEAM2[d]

[a] Ref. [40], [b] Ref. [36], [c] Ref. [41], [d] Ref. [75], [e] Ref. [76], [f] Ref. [77], [g] Ref. [78], [g] Ref. [79], [i] Ref. [80], [j] Ref. [81], [k] Ref. [82], [l] Ref. [83], [m] Ref. [84], [n] Ref. [85]

Without question, maintaining structural stability is crucial to any interatomic potentials. Therefore, the LI-EAM potentials constructed here must ensure that no unphysical structural instabilities occur not only for small but also for large deformation since they are intended for the use in atomistic simulations. We have investigated the cohesive energies of various crystal structures including bcc, fcc, hcp

with the axial ratio ranging from 1.55 to 1.7, diamond cubic, and simple cubic, under homogeneous deformation (in general not pure hydrostatic) for Li, Na, and K, as shown in Fig. 7. From this figure, it can be obviously seen that the LI-EAM potentials constructed here for Li, Na, and K metals do not favor other crystal structures over equilibrium crystal structure (i.e., bcc), even though homogeneous deformation occurs.

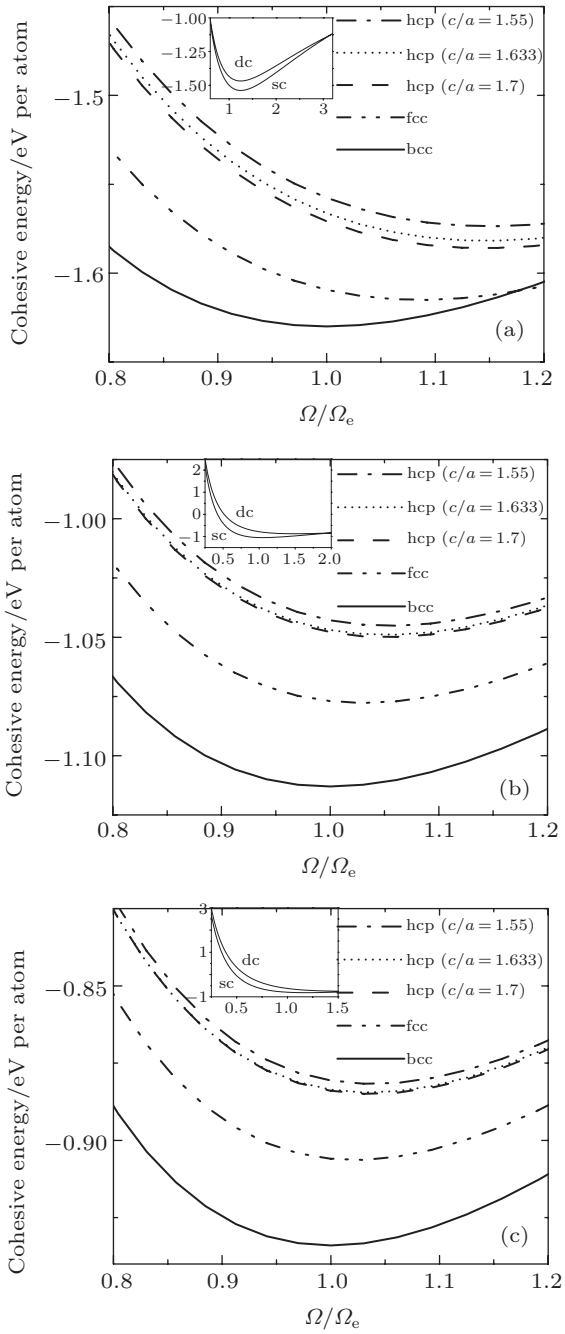


Fig. 7. The cohesive energies of various crystal structures under homogeneous deformation for (a) Li, (b) Na, and (c) K crystals.

All crystals should theoretically satisfy the following equilibrium condition:[26]

$$A_{ij} = \frac{1}{2}\sum_{m=1}^{J}\sum_{l=1}^{Z_0(m)} \frac{r_{mi\,e}^{(l)} r_{mj\,e}^{(l)}}{r_{me}} \phi'(r_{me}) = 0. \qquad (26)$$

According to the point symmetry of the crystals with fcc, bcc, and hcp structures, one can get

$$A_{ij} \equiv 0, \quad i \neq j; \quad i,j = 1,2,3. \qquad (27)$$

Then, the equilibrium condition becomes

$$A_{ii} = 0, \quad i = 1(x), 2(y), 3(z). \qquad (28)$$

For Li, Na, and K metals, the values of A_{ii} predicted with the LI-EAM potentials are displayed in Table 6. From this table, it can be seen that the values of A_{ii} are nominal, and therefore the equilibrium condition is actually satisfied for Li, Na, and K metals.

Table 6. The validation of equilibrium condition with the LI-EAM potentials for Li, Na, and K metals.

Metal	A_{xx}/eV	A_{yy}/eV	A_{zz}/eV
Li	-1.4×10^{-14}	-1.4×10^{-14}	-1.4×10^{-14}
Na	-1.8×10^{-15}	-1.8×10^{-15}	-1.8×10^{-15}
K	-5.8×10^{-16}	-5.8×10^{-16}	-6.1×10^{-16}

Among all properties considered here, it is believed that the elastic constants are those that can be measured the most accurately. Table 7 shows the elastic constants obtained with the LI-EAM potentials, via experimental measurements,[61] and from first-principles calculations[87] for Li, Na, and K. Obviously, the predicted elastic constants for Na and K metals are perfectly consistent with the experimental data. Although the predicted elastic constants for Li metal have errors of 24.9%, 14.7%, and 19.1% compared to the experimental data, they are comparable to first-principles calculations, which result in errors of 15.6%, 29.4%, and 26.4%. This suggests that the elastic constants predicted here for Li metal, as a whole, agree with the experimental data to the same extent as that calculated with first-principles. In addition, the bulk modulus and Cauchy discrepancy for Li, Na, and K metals can also be obtained directly from predicted elastic constants in Table 7, which perfectly reproduce the input values in Table 2. Incidentally, calculations with other potentials are not listed in Table 7 since all the elastic constants are used for fitting to their potential parameters in almost all other potentials.

Table 7. Comparison of the predicted elastic constants with experimental data and first-principles calculations.

Method	Li/GPa			Na/GPa			K/GPa		
	c_{11}	c_{11}	c_{44}	c_{11}	c_{12}	c_{44}	c_{11}	c_{12}	c_{44}
LI-EAM	16.8	9.76	7.10	7.71	6.06	4.03	3.7	3.12	1.86
Expt.[a)]	13.5	11.44	8.78	7.39	6.22	4.19	3.7	3.14	1.88
ab initio[b)]	15.6	14.8	11.1	–	–	–	–	–	–

[a)]Ref. [61], [b)]Ref. [87].

6. Conclusion

In this paper, it is reported that the LI-EAM interatomic potentials for Li, Na, and K, which are constructed by considering interatomic interactions up to the fourth-neighbor atoms, drastically improve the accuracy of the predicted surface energies. The predicted results agree very well with the experimental data. In addition, the predicted structural stability, elastic constants, vacancy formation and migration energies, and vacancy diffusion activation energy are satisfactorily consistent with available experimental data or first-principles calculations, and the equilibrium condition is satisfied.

References

[1] Rösch F, Rudhart C, Roth J and Trebin H R 2005 *Phys. Rev.* B **72** 014128

[2] Hocker S, Gähler F and Brommer P 2006 *Phil. Mag.* **86** 1051

[3] Ercolessi F and Adams J B 1994 *Europhys. Lett.* **26** 583

[4] Carlsson A E, Gelatt C and Ehrenreich H 1980 *Philos. Mag.* A **41** 241

[5] Wang J, Zhang K and Xie X 1994 *J. Phys.: Condens. Matter* **6** 989

[6] Yao Y and Zhang Y 1999 *Phys. Lett.* A **256** 391

[7] Chen N X, Chen Z D and Wei Y C 1997 *Phys. Rev.* E **55** R5

[8] Chen N X 2010 *Möbius Inversion in Physics* (Singapore: World Scientific Publishing) p. 183

[9] Chen N X, Shen J and Su X P 2001 *J. Phys.: Condens. Matter* **13** 2727

[10] Zhang S and Chen N X 2002 *Phys. Rev.* B **66** 064106

[11] Long Y, Chen N X and Zhang W Q 2005 *J. Phys.: Condens. Matter* **17** 2045

[12] Chen Y and Shen J 2009 *Acta Phys. Sin.* **58** 141 (in Chinese)

[13] Chen Y and Shen J 2009 *Acta Phys. Sin.* **58** 146 (in Chinese)

[14] Qian P, Liu J L, Shen J, Bai L J, Ran Q and Wang Y L 2010 *Chin. Phys.* B **19** 126001

[15] Qian P, Liu J L, Hu Y W, Bai L J and Shen J 2011 Chin. Phys. B **20** 076104

[16] Carlsson A E 1990 *Solid State Physics* (Vol. 43) (New York: Academic) pp. 1–91

[17] Daw M S and Baskes M I 1983 *Phys. Rev. Lett.* **50** 1285

[18] Daw M S and Baskes M I 1984 *Phys. Rev.* B **29** 6443

[19] Finnis M W and Sinclair J E 1984 *Philos. Mag.* A **50** 45

[20] Stillinger F H and Weber T A 1985 *Phys. Rev.* B **31** 5262

[21] Tersoff J 1986 *Phys. Rev. Lett.* **56** 632

[22] Pettifor D G 1989 *Phys. Rev. Lett.* **63** 2480

[23] Foiles S M, Baskes M I and Daw M S 1986 *Phys. Rev.* B **33** 7983

[24] Voter A and Chen S 1987 *Mater. Res. Soc. Symp. Proc.* **82** 175

[25] Johnson R A 1988 *Phys. Rev.* B **37** 3924

[26] Oh D J and Johnson R A 1988 *J. Mater. Res.* **3** 471

[27] Johnson R A and Oh D J 1989 *J. Mater. Res.* **4** 1195

[28] Adams J B and Foiles S M 1990 *Phys. Rev.* B **41** 3316

[29] Liu X Y, Adams J B, Ercolessi F and Moriarty J A 1996 *Modelling Simul. Mater. Sci. Eng.* **4** 293

[30] Liu X Y, Xu W, Foiles S M and Adams J B 1998 *Appl. Phys. Lett.* **72** 1578

[31] Mishin Y, Farkas D, Mehl M J and Papaconstantopoulos D A 1999 *Phys. Rev.* B **59** 3393

[32] Landa A, Wynblatt P, Siegel D J, Adams J B, Mryasov O N and Liu X Y 2000 *Acta Mater.* **48** 1753

[33] Li Y, Siegel D J, Adams J B and Liu X Y 2003 *Phys. Rev.* B **67** 125101

[34] Fellinger M R, Park H and Wilkins J W 2010 *Phys. Rev.* B **81** 144119

[35] Baskes M I, Srinivasan S G, Valone S M and Hoagland R G 2007 *Phys. Rev.* B **75** 094113

[36] Baskes M I 1992 *Phys. Rev.* B **46** 2727

[37] Yuan X J, Chen N X, Shen J and Hu W Y 2010 *J. Phys.: Condens. Matter* **22** 375503

[38] Sundquist B E 1964 *Acta Metall.* **12** 67

[39] Grenga H E and Kumar R 1976 *Surf. Sci.* **61** 283

[40] Guellil A M and Adams J B 1992 *J. Mater. Res.* **7** 639

[41] Hu W Y and Masahiro F 2002 *Modelling Simul. Mater. Sci. Eng.* **10** 1

[42] Daw M S 1989 *Phys. Rev.* B **39** 7441

[43] Banerjea A and Smith J R 1988 *Phys. Rev.* B **37** 6632

[44] Puska N J, Nieminen R M and Manninen M 1981 *Phys. Rev.* B **24** 3037

[45] Stott M J and Zaremba E 1982 *Can. J. Phys.* **60** 1145

[46] Rose J H, Smith J R, Guinea F and Ferrante J 1984 *Phys. Rev.* B **29** 2963

[47] Herbst J F 1981 *Phys. Rev.* B **24** 608

[48] Herbst J F and Wilkins J W 1981 *Phys. Rev.* B **24** 1679

[49] Bridgman P W 1964 *Collected Experimental Papers* (Vol. 6) (Cambridge, Massachusetts: Harvard University Press) pp. 3819, 3835

[50] Morgan A 1974 *High Temp. High Pressures* **6** 195

[51] Mao H K, Bell P M, Shaver J W and Steinberg D J 1978 *J. Appl. Phys.* **49** 3276

[52] Carter W J, Marsh S P, Fritz J N and McQueen R G 1971 *Nat. Bur. Stand. (U.S.) Spec. Publ.* **326** 147

[53] Morgan A 1975 *High Temp. High. Pressures* **7** 65

[54] Li J H, Liang S H, Guo H and Liu B X 2005 *Appl. Phys. Lett.* **87** 194111

[55] Wadley H N G, Zhou X, Johnson R A and Neurock M 2001 *Prog. Mater. Sci.* **46** 329

[56] Baskes M I 1997 *Mater. Chem. Phys.* **50** 152

[57] CASTEP (Molecular Simulation Software) 1998 http://www.accelrys.com/cerius2/castep.html

[58] Monkhorst H J and Pack J D 1976 *Phys. Rev.* B **13** 5188

[59] Barrett C S and Massalski T B 1980 *Structure of Metals* (3rd ed.) (Oxford: Pregamon Press) p. 629

[60] Kittle C 1976 *Introduction to Solid Physics* (5th ed.) (New York: John Wiley 8c Sons) p. 74

[61] Levy M, Bass H E and Stern R R 2001 *Handbook of Elastic Properties of Solids, Liquids and Gases* (vol. 2) (New York: Academic Press) pp. 99–103

[62] Vitos L, Ruban A V, Skriver H L and Kollar J 1998 *Surf. Sci.* **411** 186

[63] Baskes M I 1992 *Phys. Rev.* B **46** 2727

[64] Foiles S M 1987 *Surf. Sci.* **191** L779

[65] Dai X D, Li J H and Kong Y 2007 *Phys. Rev.* B **75** 052102

[66] Li J H, Kong Y, Guo H B, Liang S H and Liu B X 2007 *Phys. Rev.* B **76** 104101

[67] Hu W Y, Zhang B W, Huang B Y, Gao F and Bacon D J 2001 *J. Phys.: Condens. Matter* **13** 1193

[68] Hu W Y, Shu X L and Zhang B W 2002 *Comput. Mater. Sci.* **23** 175

[69] Hu W Y, Deng H Q, Yuan X J and Fukumoto N 2003 *Eur. Phys. J.* B **34** 429

[70] Zhang B W, Hu W Y and Shu X L 2003 *Theory of Embedded Atom Method and its Applications to Materials Science–Atomic Scale Materials Design Theory* (Changsha: Hunan University Press)

[71] Ackland G J and Finnis M W 1986 *Philos. Mag.* A **54** 301

[72] Wang Y R and Boercker D B 1995 *J. Appl. Phys.* **78** 122

[73] Zope R R and Mishin Y 2003 *Phys. Rev.* B **68** 024102

[74] Mishin Y, Asta M and Li J 2010 *Acta Materialia* **58** 1117

[75] Ouyang Y F, Zhang B W and Liao S Z 1994 *Sci. China* A **37** 1232

[76] Feder R 1970 *Phys. Rev.* B **2** 828

[77] Shultz H 1991 *Landolt-Bornstein, New Series, Group III* (vol. 25) (Berlin: Springer)

[78] Frank W, Breier U, Elsasser C and Fahnle M 1993 *Phys. Rev.* B **40** 7676

[79] Messer R and Noack F 1975 *Appl. Phys.* **6** 79

[80] Schott V, Fahnle M and Madden P A 2000 *J. Phys.: Condens. Matter* **12** 1171

[81] Schober H R, Petry W and Trampenau J 1992 *J. Phys.: Condens. Matter* **4** 9321

[82] Feder R and Charbnau H P 1966 *Phys. Rev.* **149** 464

[83] Crawford J H and Slifkin L M 1972 *Point Defects in Solids: General and Ionic Crystals* (vol. 1) (New York: Plenum Press) p. 54

[84] Damak A C and Dienes G J 1963 *Point of Defects in Metals* (New York: Science Publishers Inc.) pp. 195–208

[85] Madonald R A, Shukla R C and Kahaner D K 1984 *Phys. Rev.* B **29** 6489

[86] Harder J M and Bacon D J 1986 *Philos. Mag.* A **54** 651

[87] Mehl M J 1993 *Phys. Rev.* B **47** 2493